Developmental Cognitive Neuroscience 30 (2018) 223–235

Contents lists available at ScienceDirect

Developmental Cognitive Neuroscience

journal homepage: www.elsevier.com/locate/dcn

The development of functional network organization in early childhood and early adolescence: A resting-state fNIRS study

Lin Cai[a,b,c], Qi Dong[a,b,c], Haijing Niu[a,b,c,*]

[a] State Key Laboratory of Cognitive Neuroscience and Learning, Beijing Normal University, Beijing, 100875 China
[b] IDG/McGovern Institute for Brain Research, Beijing Normal University, Beijing, 100875 China
[c] Center for Collaboration and Innovation in Brain and Learning Sciences, Beijing Normal University, Beijing, 100875 China

ARTICLE INFO

Keywords:
Brain development
Connectome
Brain networks
fNIRS
Resting state

ABSTRACT

Early childhood (7–8 years old) and early adolescence (11–12 years old) constitute two landmark developmental stages that comprise considerable changes in neural cognition. However, very limited information from functional neuroimaging studies exists on the functional topological configuration of the human brain during specific developmental periods. In the present study, we utilized continuous resting-state functional near-infrared spectroscopy (rs-fNIRS) imaging data to examine topological changes in network organization during development from early childhood and early adolescence to adulthood. Our results showed that the properties of small-worldness and modularity were not significantly different across development, demonstrating the developmental maturity of important functional brain organization in early childhood. Intriguingly, young children had a significantly lower global efficiency than early adolescents and adults, which revealed that the integration of the distributed networks strengthens across the developmental stages underlying cognitive development. Moreover, local efficiency of young children and adolescents was significantly lower than that of adults, while there was no difference between these two younger groups. This finding demonstrated that functional segregation remained relatively steady from early childhood to early adolescence, and the brain in these developmental periods possesses no optimal network configuration. Furthermore, we found heterogeneous developmental patterns in the regional nodal properties in various brain regions, such as linear increased nodal properties in the frontal cortex, indicating increasing cognitive capacity over development. Collectively, our results demonstrated that significant topological changes in functional network organization occurred during these two critical developmental stages, and provided a novel insight into elucidating subtle changes in brain functional networks across development.

1. Introduction

Recent findings from behavioral and brain imaging studies have demonstrated that the enhancement of cognitive processes during normal brain development involves a fine-tuning of structural and functional organization of the brain from birth to adulthood (Collin and van den Heuvel, 2013; Giedd et al., 1999; Hagmann et al., 2012; Sowell et al., 2003; Vertes and Bullmore, 2015). According to Piaget's theory of cognitive development (Piaget, 1999), early childhood (7–8 years old) is a critical period during which young children undergo the transition from the preoperational stage to the concrete operational stage. Specifically, they start thinking logically about concrete events and solving problems in a more logical manner, but their thinking remains very concrete. Additionally, although numerous important cognitive functions, such as attention, memory and inhibitory control, develop quickly, they are nonetheless less developed (Brocki and Bohlin, 2004; Davidson et al., 2006; Schneider and Ornstein, 2015). Early adolescence (11–12 years old) constitutes the starting point of the formal operational stage. In this stage, adolescents can use symbols related to abstract concepts to accomplish hypothetical and deductive reasoning, which benefits from improved working memory and executive inhibitions at this critical developmental stage (Bedard et al., 2002; Ernst and Mueller, 2008; Gathercole et al., 2004; Williams et al., 1999). These dramatic improvements of cognitive performance from early childhood to early adolescence may imply significant increases in the brain's efficiency with development. However, few studies have investigated the developmental topological characteristics of brain functional networks during these two critical periods.

The human brain constitutes an integrative, complex network system with numerous non-trivial local and global topological

* Corresponding author at: State Key Laboratory of Cognitive Neuroscience and Learning, Beijing Normal University, Beijing 100875, China.
E-mail address: niuhjing@bnu.edu.cn (H. Niu).

https://doi.org/10.1016/j.dcn.2018.03.003

Available online 08 March 2018

characteristics, which can be examined by graph theory (Bullmore and Sporns, 2009). A network's topological patterns are evaluated using the key properties of graph theory, such as clustering coefficient, characteristic path length, node degree, efficiency, and modularity (Sporns and Zwi, 2004) (see Section 2.6 for details). The clustering coefficient of a graph provides information about the level of local clustering within a graph, expressing how well the neighbors of a node are connected amongst themselves. This offers a measure of how much spatially-closer brain regions are connected with each other, or the local connectedness of the network. The level of global connectivity of the network can be assessed with the characteristic path length of a graph, which describes how close, on average, a node of the network is connected to every other node in the network. This provides information on how efficiently information can be integrated between different subgraphs. The degree of a node describes the number of connections of a node and offers information about the existence of highly connected hub nodes in the brain network. Nodes with a high nodal efficiency indicate that the network has a high tolerance for the elimination of a given node, which is associated with a high clustering of the neighborhood of this node (Achard and Bullmore, 2007). The level of modularity of a network describes the extent that groups of nodes in the graph are connected to other members of their own group, establishing sub-networks within the greater network. Taken together, these metrics of graph theory provide critical information about the structure of a network and characterize a specific organization style (e.g., small-world, modular) of that network.

Fair et al. (2009) applied resting-state functional connectivity and graph theory to investigate the topological organization of the developing brain in three age groups (aged 7–9, aged 10–15, aged 19–31). Their study revealed that children and adults have similar clustering coefficients and characteristic path lengths, but different spatial distributions of modularity organization throughout development (Fair et al., 2009). Furthermore, by comparing the organization of brain networks between 7–9 year old children and adults, Supekar et al. (2009) determined that children's and young adults' brains have a similar small-world regime, and demonstrated simultaneous reduction of short-range functional connectivity and strengthening of long-range functional connectivity from childhood to adulthood. A recent study over the age range of 6–18 years reported increases in the normalized clustering coefficient, local efficiency and small-worldness, but global efficiency was not significantly changed with development (Wu et al., 2013). The findings were further supported by a lifespan study (Cao et al., 2014) that demonstrated that local efficiency increased slightly from early childhood to early adulthood (7–30 years). To date, almost all extant literature focusing on topological developmental changes in functional networks has been performed over a relatively broad age range (Cao et al., 2014; Fair et al., 2009; Supekar et al., 2009; Wu et al., 2013). These combined results suggest that graph theoretical analysis constitutes a powerful tool to characterize the topological development of functional brain networks.

Since almost all relevant previous studies have considered a relatively wide age range, a refined examination of two relatively narrow and critical developmental periods is worthy of investigation. We predicted that the functional difference between two noncontiguous age groups will offer non-trivial insight for normal child development and a valuable reference for the clinical diagnosis of psychopathology across development. More importantly, in the current study, we adopted resting-state functional near-infrared spectroscopy (rs-fNIRS) to address the developmental changes of brain networks. Compared with functional magnetic resonance imaging (fMRI), fNIRS is silent and more tolerant to subtle movement artifacts, and can measure both oxy- and deoxy-hemoglobin chromophores, providing a more comprehensive measure of cortical hemodynamic response. Furthermore, it is generally acceptable for children to participate in fNIRS studies because data acquisition is performed in a natural environment. (Bunge and Wright, 2007; Davidson et al., 2006). In addition, compared to fMRI imaging, fNIRS has much better temporal resolution, up to hundreds of hertz, thus providing a more complete temporal picture for the characterization of brain activity (Lloyd-Fox et al., 2010).

In the present study, we utilized rs-fNIRS to examine developmental changes in both global and regional nodal topological properties from early childhood and early adolescence to adulthood. We hypothesized that from early childhood to early adolescence, there would be a significant linear improvement in certain topological characteristics of brain networks, such as local and global efficiency, revealing functional segregation and integration. Additionally, we predicted that diverse developmental trajectories in different functional cortices would be found throughout development.

2. Materials and methods

2.1. Participants

This study enrolled 90 healthy participants, including 30 young children (age range of 7.0–8.9 years old with mean and standard deviation of 8.1 ± 0.6 years; 14 M/16 F), 30 early adolescents (age range of 11.0–12.9 years old with mean and standard deviation of 11.9 ± 0.6 years; 19 M/11 F), and 30 adults (age range of 19–27 years old with mean and standard deviation of 23.2 ± 1.9 years; 16 M/14 F). All participants were right-handed as assessed by the Edinburgh Handedness Inventory (Oldfield, 1971). The participants or their parents signed a written informed consent form prior to the initiation of the experiments. Approval for this study was obtained from the Institutional Review Board of the State Key Laboratory of Cognitive Neuroscience and Learning, Beijing Normal University.

2.2. Data acquisition

Each participant's hemodynamic response was recorded using a continuous wave near-infrared optical imaging system (CW6, TechEn Inc., MA, U.S.A.) equipped with 12 light sources and 24 detectors at 690 nm and 830 nm wavelengths. The light sources and detectors were placed on a stretchable cap, forming 46 measurement channels (source–detector separation: 3.2 cm) and covering almost the whole head (Fig. 1A, B). The positioning of the probe array was determined according to the international 10–20 coordinate system, and referred to the external auditory canals and vertex of each participant as landmarks. Specifically, six detectors below channels 17–24 in both hemispheres were set along a coronal line from the vertex to the external auditory pores, and thus their midline was localized in Cz and the leftmost and rightmost detectors were fitted around T3 and T4, respectively. Data were recorded at a sampling rate of 50 Hz. For each participant, the rs-fNIRS data were collected for approximately 11 min, and the participants were instructed to relax, keep their eyes closed, and remain awake.

2.3. MRI coregistration

To validate the positioning method of the probes, a structural MR image was acquired from one arbitrarily selected adult subject (SJ). During MRI data acquisition, the participant lay supine while wearing the probe array. The probe array was pasted with vitamin E capsules placed precisely at each of the optode locations. All scans were performed using a 3T Siemens Tim Trio MRI scanner at the Imaging Center for Brain Research, Beijing Normal University. The vitamin E locations from these scans were used as landmarks for coregistration (Fig. 1C). A T1-weighted structural image was acquired using a magnetization-prepared rapid gradient echo (MPRAGE) sequence: 176 slices, TR = 2600 ms, TE = 3.02 ms, FOV = 256 × 224 mm^2, voxel size = 1 mm × 1 mm × 1 mm, flip angle = 8°, and slice orientation = sagittal. The MR image was normalized into MNI space using the NIRS_SPM software (http://bispl.weebly.com/nirs-spm.html#/), and

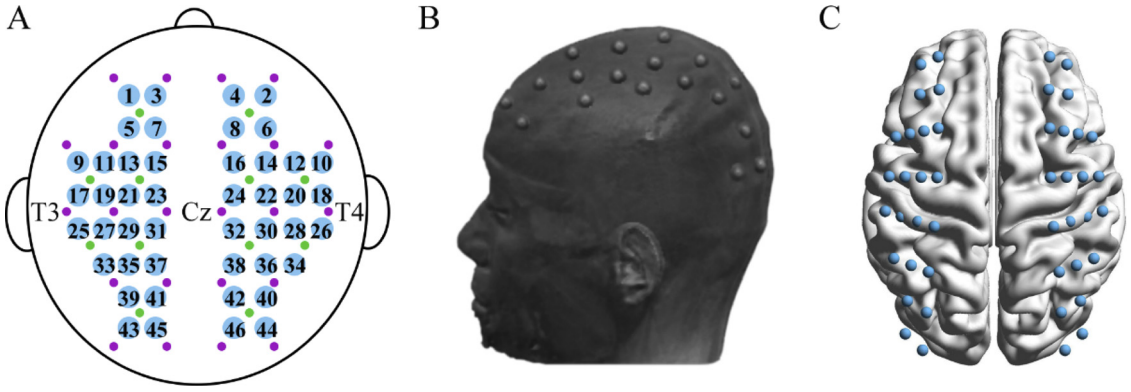

Fig. 1. fNIRS data collection and MRI Neuroanatomical Co-Registration. (A) The arrangement of the 46 measurement channels across the whole head. The green and purple dots represent the sources and detectors, respectively. The digits represent the positions of the measurement channels. (B) MRI co-registration was conducted by asking a participant to wear probe arrays with vitamin E capsules in MRI. (C) The anatomical position corresponding to each measurement channel. (For interpretation of the references to colour in this figure legend, the reader is referred to the web version of this article.)

the Montreal Neurological Institute (MNI) coordinates for each measurement channel were determined according to the automated anatomical labeling (AAL) template (Tzourio-Mazoyer et al., 2002). A similar positioning method can be found in previous fNIRS studies (Kovelman et al., 2008; Kovelman et al., 2009; Sasai et al., 2012). For the cortical position corresponding to each measurement channel, see Table S1 in Supplementary Materials.

2.4. Data preprocessing

We evaluated the relative changes in oxy-hemoglobin (HbO) and deoxy-hemoglobin (HbR) concentration on an arbitrarily assigned zero baseline from the start of the measurement period, which was based on the modified Lambert–Beer law (Cope and Delpy, 1988). For the time course of the HbO and HbR signals, we first conducted a temporal independent component analysis (ICA) to remove typical motion-induced artifacts and systematic physiological noise (Niu et al., 2013). This analysis procedure was performed by using a publicly available software, *FastICA v2.5* (www.cis.hut.fi/projects/ica/fastica/). Specifically, the ICA analysis was separately performed on the raw data of HbO and HbR with the following procedures: 1) extracting steady hemoglobin concentration signals (i.e., removing the initial time points from total data length); 2) reducing the dimensionality of the data with principal component analysis; 3) performing ICA analysis on the reduced dimensional data; 4) identifying noise components; 5) removing noise from the measured data and calculating "real" neural activity signals. After ICA analysis, the components related to motion-induced artifacts and physiological noise were identified from three aspects: temporal profiles, spatial maps, and power spectra. A component was treated as noise if it met one of the following criterion (Zhang et al., 2010): 1) the corresponding temporal profile included sudden jumps, slowly varied U or inverted U-shaped spike, or numerous inter-current quick spikes; 2) the dominant frequency of power spectra of the component was outside the range of 0.01–0.1 Hz; or 3) the spatial map of the component presented a global and spatially dispersive pattern. After identifying these types of noise components, each concentration signal of HbO and HbR was reconstructed with a particular component eliminated from the original rs-fNIRS time course by replacing zero in the corresponding column of the mixing matrix (Kohno et al., 2007). Then, we adopted a band-pass filtering with cutoff frequencies of 0.009 and 0.08 Hz to reduce the effect of high-frequency noise and baseline drift, and to obtain the low frequency hemodynamic signals that emanated from spontaneous neural activity (Biswal et al., 1995; Sasai et al., 2012; White et al., 2009). Finally, we extracted 10-min data, including 30,000 sample points, from the continuous time course of each participant to perform the network topology analyses. The data preprocessing was conducted using in-house FC-NIRS package (http://www.nitrc.org/projects/fcnirs; Xu et al. (2015)), which was developed using MATLAB 2010b (www.mathworks.org) in a 64-bit Windows 7 environment. In the current study, we mainly used HbR signals to characterize topological development of functional brain networks, considering that HbR has been demonstrated in our previous study (Niu et al., 2013) to have an overall much higher reliability for most brain network metrics and consistently considered as the physiological basis of the fMRI BOLD signals (Buxton et al., 1998; Ogawa et al., 1993). The brain development results derived from the HbR signals also allow us to make a direct comparison with those derived from fMRI. As a complement, HbO signals were also utilized in our study to investigate the topological development of functional brain networks. The HbO results were included in the Supplementary Materials.

2.5. Network construction

The application of graph theory to construct human brain functional networks extracted from functional imaging data requires two steps to be performed. First, the nodes should be defined. Second, the strength of the connections between any two nodes needs be quantified by similarity measures (e.g., Pearson correlation) between their respective time series above a threshold. If the strength of the connections exceeds the predefined threshold, the connections are treated as the edges of a graph. These two steps are important since the definition of the nodes and the edges determines the network properties that are then used for neurobiological interpretation (Rubinov and Sporns, 2010). Commonly applied thresholding methods include correlation-based and sparsity-based methods. Correlation-based method generally sets a value for the correlation coefficient between node pairs, above which they are considered connected and below which they are not. This method will result in different numbers of edges due to differences in the low-level correlations among different groups. In contrast, sparsity-based thresholds generally define network sparsity as the ratio of the number of existing edges divided by the maximum possible number of edges in a network. For group comparisons, this method can ensure that the networks have the same number of edges or wiring cost for each group (Achard and Bullmore, 2007; Stam et al., 2007). Therefore, in the current study, we adopted the sparsity-based method to construct brain network and then to conduct group comparison of topological development of brain networks.

In the current study, we used MATLAB (www.mathworks.org) functions from the GRETNA toolbox (http://www.nitrc.org/projects/gretna; Wang et al., 2015) to construct the brain functional network for each subject. For each individual rs-fNIRS data set, we obtained a 46×46 symmetric correlation matrix by calculating Pearson correlation coefficients between the time series of every pair of nodes in which the nodes were the measurement channels. Due to the ambiguous

biological explanation of negative correlations (Fox et al., 2009; Murphy et al., 2009), we replaced all negative correlation coefficients to zero and restricted our analysis to positive correlations. These correlation coefficients were then converted to Z-values via Fisher's *r*-to-*z* transformation to improve normality, resulting in a 46 × 46 Z-value functional connectivity matrix Z_{ij} for each subject, where $i, j = 1, 2, \ldots 46$. Each functional connectivity matrix can be converted to a binarized B_{ij} using a sparsity threshold, where B_{ij} is 1 if the value of the Z-value functional connectivity matrix Z_{ij} between regions i and j is larger than a given sparsity threshold, and 0 otherwise. To perform a group-averaged functional connectivity comparison, the individual Z-value functional connectivity matrices were first averaged within each age group, and then the group-level Z-value matrix was converted into an R-value matrix via Fisher's *z*-to-*r* transformation for each age group, respectively. Of note, the main network analyses were based on binary brain networks. However, the effects of other sparsity thresholds and weighted network analysis on our results were also evaluated (see the following Section 2.8 "Validation").

2.6. Network analysis

Graph theory was utilized to describe the topological organization of the human brain functional networks. Similar to earlier studies (Bassett et al., 2008), the correlation matrix was thresholded over a range of sparsity (5% < s < 25%, stepsize = 1%) in order to investigate the relationship between sparsity and the network properties. Meanwhile, we also adopted a single sparsity (s = 20%) to normalize all of the networks to have the same number of edges, and thus to explore the between-group differences in the same-size network topological organization. These network metrics are explained as follows:

2.6.1. Global network metrics

Six global network metrics, including the normalized clustering coefficient (C_p), characteristic path length (L_p), global efficiency (E_{glob}), local efficiency (E_{loc}), small-worldness (σ), and modularity (Q) were used to elucidate global topological organizational changes in the developing brain (for illustrations, see Fig. 2) (Fair et al., 2009; Fan et al., 2011). Their definitions and descriptions can be found as follows, and in Rubinov and Sporns (2010).

For graph G with N nodes and K edges, the clustering coefficient C_p of the graph G is calculated as follows (Watts and Strogatz, 1998):

$$C_p = \frac{1}{N}\sum_{i\in G}\frac{E_i}{D_i(Di-1)/2}$$

where D_i denotes the number of edges connected to node i; and E_i is the number of edges in the subgraph, including the neighbors of node i. The clustering coefficient reflects the local interconnectivity and cliquishness of a network.

The characteristic path length L_p of graph G is defined as the average of the shortest path lengths between all pairs of nodes in network G (Watts and Strogatz, 1998):

$$L_p = \frac{1}{N(N-1)}\sum_{i\neq j\in G} d_{ij}$$

where d_{ij} is the shortest path length between node i and node j. The shortest path length was the minimum number of edges included in the path that connected these two nodes. The characteristic path length measures the ability of parallel information propagation (Latora and Marchiori, 2003).

To examine the small-world attributes of a network, the normalized clustering coefficient $\gamma = C_p^{real}/C_p^{rand}$ and the normalized characteristic path length $\lambda = L_p^{real}/L_p^{rand}$ were computed (Watts and Strogatz, 1998). C_p^{real} and L_p^{real} are the clustering coefficient and the characteristic path length of a real network, respectively, and C_p^{rand} and L_p^{rand} represent the means of the corresponding parameters derived from 1000 matched random networks that have the same numbers of nodes, edges, and distribution of degrees as the real brain network. Typically, a small-world network should meet the following criteria: $\gamma > > 1$ and $\lambda \approx 1$ (Uehara et al., 2014).

In addition to the conventional small-world parameters (C_p and L_p), the more biologically relevant properties of brain networks are efficiency parameters, including global efficiency and local efficiency, which measure the capability of the network with regard to information transmission at the global and local levels, respectively. Global efficiency E_{glob} is defined as the inverse of the harmonic mean of the shortest path length between any two nodes (Latora and Marchiori, 2001):

$$E_{glob} = \frac{1}{N(N-1)}\sum_{i\neq j\in G}\frac{1}{d_{ij}}$$

where d_{ij} is the shortest path length between node i and node j.

Local efficiency E_{loc} of a network G is defined as the average of the local efficiencies of all nodes, where the local nodal efficiency for a given node i is the global efficiency of the subgraph composed of the nearest neighbors to node i (Achard and Bullmore, 2007; Latora and Marchiori, 2001):

$$E_{loc} = \frac{1}{N}\sum_{i\in G} E_{glob}(i)$$

where $E_{glob}(i)$ is the global efficiency of G_i, which is the subgraph of the neighbors of node i. The use of global efficiency is more advantageous than the use of the characteristic path length, particularly in the case of disconnected networks, because the disconnected nodes are considered to have an infinite path length and a corresponding zero efficiency.

Modularity reflects the degree to which a network is organized into a modular or community structure (Newman, 2006). For a given partition p of a network, the modularity is defined as follows:

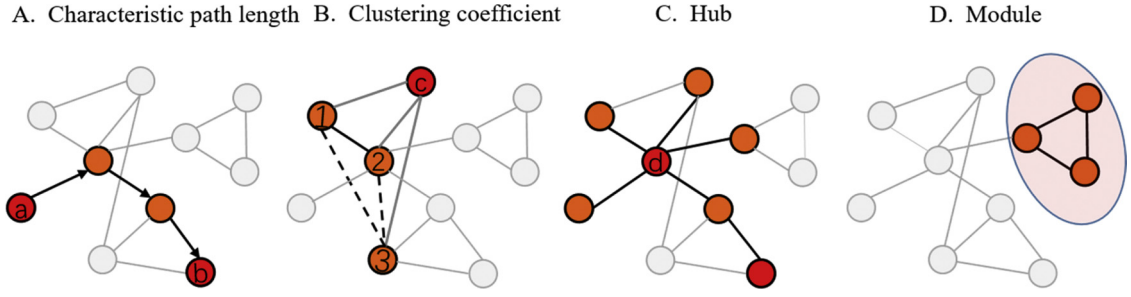

Fig. 2. The topological properties of networks. We illustrate the topological properties of networks by a network composed of 10 nodes and 13 edges. (A) The characteristic path length between nodes a and b is the shortest path length, as indicated by the three black arrow lines. (B) The clustering coefficient of node c is the number of existing connections (i.e., 1–2) among the node's neighbors divided by all of their possible connections (i.e., 1–2, 1–3, 2–3), which is 1/3 (the dashed lines indicate the absence of a connection between the neighbors of node c). (C) Shows a network with a highly connected hub node d, which plays a central position in the overall network. (D) Shows the presence of a clustered module, as indicated by the three nodes (encircled in pink) being mutually strongly interconnected, but sparsely connected to the rest of the network.

$$Q(p) = \sum_{M}^{m-1} \left[\frac{l_m}{L} - \left(\frac{d_m}{2L} \right)^2 \right]$$

where M is the number of modules; L is the number of connections in the network; l_m is the number of connections between the nodes in module m; and d_m is the sum of the degrees of the nodes in module m. The modularity attempts to partition the graph into disconnected subgraphs to minimize the degree of inter-module connectivity and maximize intra-module connectivity.

2.6.2. Regional nodal metrics

Regional topological characteristics were evaluated in terms of nodal degree and nodal efficiency. The degree of a given node i is defined as the number of edges linked to the node as:

$$K_{nod}(i) = \sum_{j \neq i \in G} a_{ij},$$

where a_{ij} is the i^{th} row and j^{th} column element in the formerly obtained adjacency matrix.

The efficiency of node i is measured as follows:

$$E_{nod}(i) = \frac{1}{N-1} \sum_{j \neq i \in G} \frac{i}{d(i,j)},$$

where $d(i,j)$ is the shortest path length between node i and node j. Nodes with a high nodal efficiency indicate that the network has a high tolerance to the elimination of a given node, which is associated with a high clustering of the neighborhood of this node (Achard and Bullmore, 2007). In addition, we employed nodal degree and nodal efficiency to identify functional hubs across three age groups, respectively. The nodes with higher values in nodal degree and nodal efficiency (at least 1 standard deviation greater than the average of all nodes in the network) were defined as brain hubs, which are usually assumed to play central roles in the functional integrity of whole brain networks. BrainNet Viewer (http://www.nitrc.org/projects/bnv/) was used for visualization of regional nodal properties.

2.7. Statistical analysis

To characterize the developmental changes in global topological properties, we separately performed one-way analysis of variance (ANOVA) on the three age groups for each global metric. Tukey's honest significant difference (HSD) tests were applied as *post hoc* tests. Furthermore, to guarantee the statistical reliability of the obtained findings, a bootstrap analysis of the confidence intervals was conducted using 1000 bootstrap samples. For the global network properties, confidence intervals (95%) for each topological property among these three age groups were calculated from the bootstrap values, and the differences among the groups were determined by the lack of overlap in these confidence intervals (Garrett et al., 2013).

To determine the developmental changes in regional nodal properties from early childhood, early adolescence to adulthood, a general linear model (GLM) was utilized for each nodal metric. Specifically, to explore linear or quadratic age effects, we used two multiple linear regressions that modeled each nodal metric with age or age^2 as predictors. The GLM models were separately formulated as follows:

$$Y = \beta_0 + \beta_1 \times \text{age} + \text{e}$$

$$Y = \beta_0 + \beta_1 \times \text{age} + \beta_2 \times \text{age}^2 + e$$

We adopted a finite sample corrected Akaike's information criterion (AIC), namely, AICc (Hurvich and Tsai, 1989), to determine the best model among the two regressions. AIC reflects a trade-off between the likelihood and complexity (i.e., number of parameters) of a model. The regression model with the lowest AICc value was chosen as the best model to fit the data. Multiple comparisons among channels were considered by adopting Bonferroni correction for HbO data and the false discovery rate (FDR) correction at $q < 0.05$ (Benjamini and Hochberg, 1995) for HbR data.

2.8. Validation

Considering that network sparsity thresholds and different network construction approaches may influence the reproducibility of the network topological attributes derived from the rs-fNIRS data, we performed additional complementary analyses. On the one hand, we recomputed the developmental changes in the global topological properties and regional nodal properties using two other sparsity thresholds (i.e., 15% and 25%) and then performed the statistical analyses. On the other hand, weighted networks were computed to validate the reproducibility of our results. Moreover, we also used HbO signals to examine the effect of different hemoglobin concentration signals on our main results.

3. Results

3.1. Functional connectivity

We showed the functional connectivity pattern at the group level for young children, early adolescents, and adults, respectively (Fig. 3). We determined that the functional connectivity correlation coefficients in young children (mean ± SD = 0.23 ± 0.01) and early adolescents (mean ± SD = 0.18 ± 0.01) had a shorter tail of positive correlations compared to those in the adult group (mean ± SD = 0.13 ± 0.02). Young children and early adolescents also exhibited similar functional connectivity organization as that in adults, i.e., high correlations between the contralateral homologous regions and the neighboring ipsilateral regions.

3.2. Economic small-world organization

Fig. 4 shows the profiles of six global parameters calculated from both the real brain network (warm colors) and random networks (cold colors), and shown as functions of the sparsity thresholds. We found that in the sparsity range of 5% ~ 25%, the C_p values of brain functional networks were larger than those of the matched random networks (Fig. 4A), and the L_p values were comparable to those of the matched random networks (Fig. 4B). When evaluating the small-worldness, we observed that the small-worldness values were larger than 1 in the sparsity range of 5% ~ 25% in all three age groups (Fig. 4C). Thus, these network organizations for each age group reflect typical features of small-world topology, demonstrating a balance between local segregation and global integration in the developing brain. From the perspective of the efficiency, the local efficiency of the networks was larger than that of the matched random networks (Fig. 4E), whereas the global efficiency of the networks was comparable to that of the matched random networks (Fig. 4D). These results further supported the small-worldness organization of the brain networks, which are approximately efficient in global information processing, but more efficient in local information processing compared with the matched random networks. Furthermore, the functional brain networks in these three age groups consistently showed a higher modularity compared with that derived from the matched random networks (Fig. 4F). These combined results demonstrated that functional brain connectivity networks in young children and early adolescents have been specially organized according to non-trivial wiring principles.

3.3. Developmental changes in global network properties

One-way ANOVAs were utilized to conduct the developmental comparison in network topological measures among the age groups. With development, significant age effects were found on the normalized C_p ($F_{(2,87)} = 5.15$, $p = 0.008$), small-worldness ($F_{(2,87)} = 3.45$,

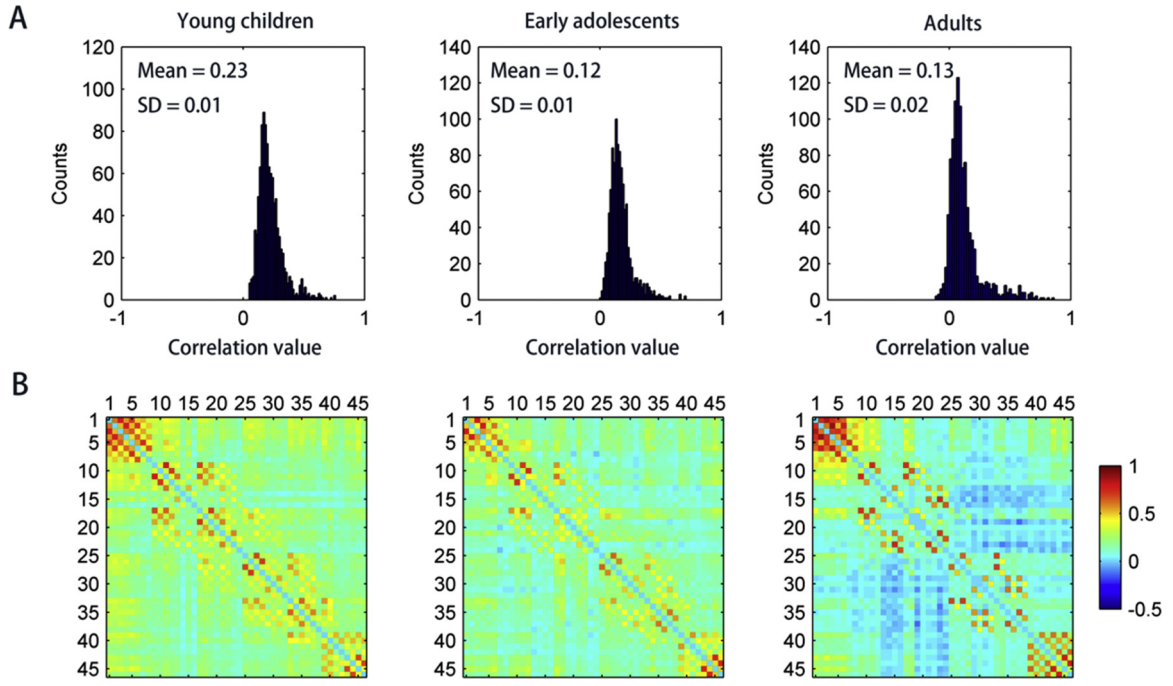

Fig. 3. The distribution of r values within the raw r value correlation matrices of three age groups (A). The averaged population-level correlation matrices of three age groups (B) (digits in matrices represent measurement channels).

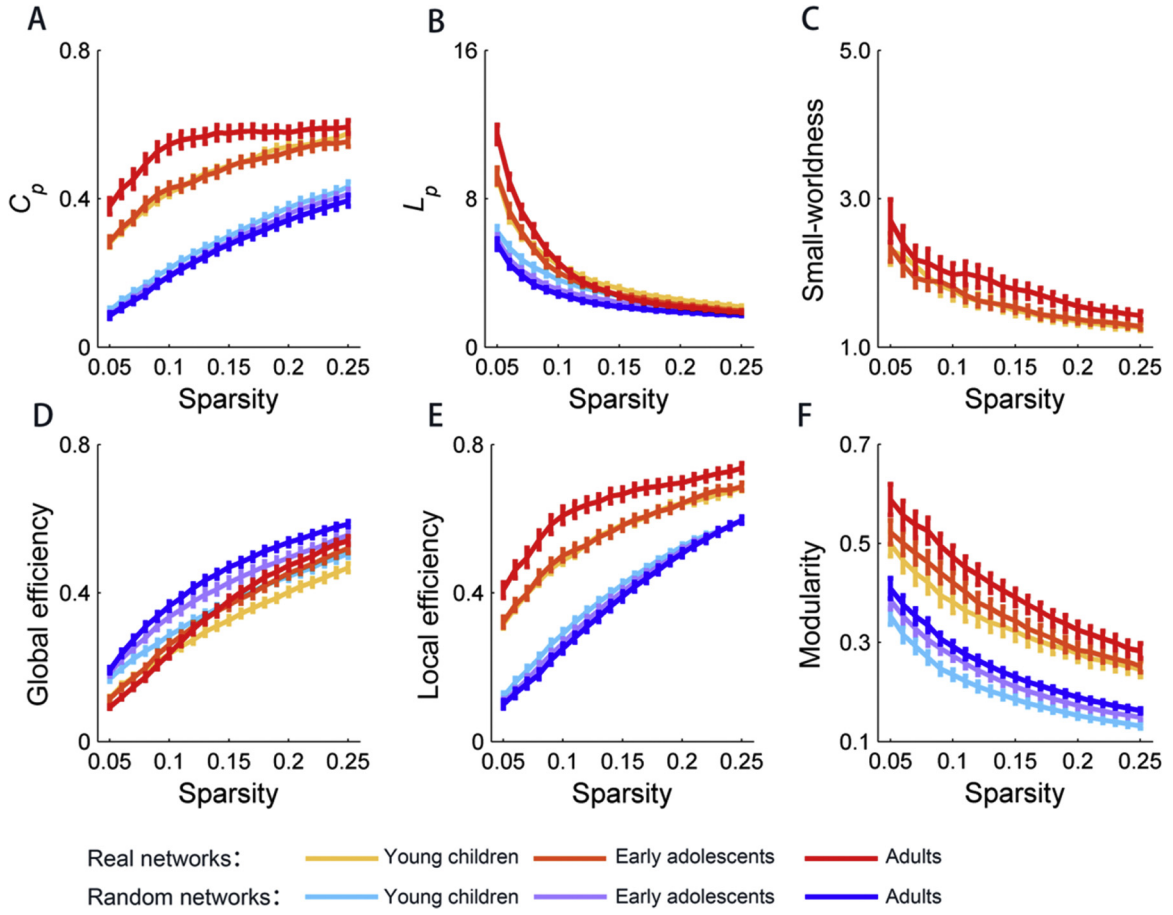

Fig. 4. The global network metrics in a range of sparsity thresholds (5%–25%). (A) The clustering coefficient and (B) the characteristic path length are shown as a function of the sparsity thresholds compared with the matched random networks. (C) The small-worldness is shown as a function of the sparsity thresholds. (D) Global efficiency, (E) local efficiency, and (F) modularity are presented as a function of the sparsity thresholds compared with the matched random networks. Error bars (A, B, D, E, F) correspond to the standard errors of the mean for 1000 comparable random null networks. Error bars in (C) indicate the standard errors in all subjects.